PR12-17-005

The CaFe Experiment: Isospin Dependence of Short-Range Nucleon Pairing in Nuclei Proposal to Jefferson Lab PAC 45

F. Hauenstein, C.E. Hyde, M. Khachatryan, H. Szumila-Vance, L.B. Weinstein (co-spokesperson)
Old Dominion University, Norfolk VA

K. Allada, W. Bertozzi, S. Gilad, O. Hen (contact person), A Papadopoulou,
A. Schmidt, B.A. Schmookler, E.P. Segarra, and R. Cruz Torres
Massachusetts Institute of Technology, Cambridge, MA

E.O. Cohen (co-spokesperson), M. Duer, J. Lichtenstadt, E. Piasetzky, and O. Reich
Tel-Aviv University, Tel Aviv, Israel

J. Bericic, S.C. Dusa, S. Glamazdin, D.W. Higinbotham (co-spokesperson), E. McClellan, D. Meekins, and B. Sawatsky
Thomas Jefferson National Accelerator Facility, Newport News, VA

J.R.M. Annand, D.J. Hamilton, and R. Montgomery
University of Glasgow, Scotland UK.

T. Brecelj, M. Mihovilovič, S. Širca, S. Štajner Jožef Stefan
Institute and University of Ljubljana, Slovenia

A. Beck, I. Korover, and S. Maytal-Beck
Nuclear Research Center Negev, Beer-Sheva, Israel

S. Wells, N. Simicevic, and R. Beminiwattha
Louisiana Tech University, Ruston, LA

M. Kohl, N. Kalantarians, A. Liyanage, B. Dongwi, J. Nazeer
Hampton University, Hampton, VA

P.E.C. Markowitz
Florida International University, Miami, FL

E. Long
University of New Hampshire, Durham, NH

K. Aniol
California State University, Los Angeles, CA

F. Benmokhtar
Duquesne University, Pittsburgh, PA

D. Androic
University of Zagreb, Bijenicka, Zagreb

S. Danagoulian
North Carolina A&T State University, Greensboro, NC

W. Tireman
Northern Michigan University, Marquette, MI
(Dated: May 21, 2017)

Abstract

Short-Range Correlations (SRCs) are the term used to describe pairs of nucleons with large relative momenta and small center-of-mass momenta compared to the nuclear Fermi momentum (k_F). Recent studies indicate that SRCs account for 20–25% of the nucleons in medium to heavy nuclei, make up essentially all nucleons with momentum greater than k_F, and contribute most of the kinetic energy carried by nucleons in nuclei. Based on these and other findings, recent works found intriguing implications of SRCs for bound nucleon structure functions and the EMC effect, two-nucleon knockout processes in neutrino-nucleus scattering measurements, the density dependence of the nuclear symmetry energy and more.

Some of the most intriguing SRC results that have come out of the JLab 6 GeV era have been related to asymmetric nuclei, specifically that in neutron-rich nuclei, protons can have large average kinetic energy compared to neutrons, despite being the minority species. The current best data are limited, however. The myriad of (e, e') measurements on different nuclear targets do not allow separation of proton and neutron contributions. The existing semi-inclusive and exclusive measurements only cover a few species—either light symmetric nuclei, or a few heavy elements— preventing a systematic study of the nuclear mass and proton-neutron asymmetry dependencies.

We propose to systematically study the individual probabilities for finding SRC protons and neutrons in neutron-rich symmetric and asymmetric nuclei (d, ^{4}He, ^{9}Be, ^{10,11}B, ^{12}C, ^{28}Si, ^{40}Ar, ^{40,48}Ca, ^{48}Ti and ^{54}Fe), complementing the approved 12 GeV inclusive EMC and SRC experiments on the same nuclei. To this end, we propose measuring the $(e, e'p)$ reaction in kinematics dominated by scattering off mean-field ($k \leq k_F$) and SRC pairs ($k \geq k_F$). We will extract absolute and reduced cross sections (distorted spectral functions) and cross-section ratios as a function of missing energy and momentum. The measurement results will be used to determine the separate SRC pairing probabilities for protons and neutrons in order to determine how pairing depends on nuclear mass and proton-neutron asymmetry. These probabilities will also be directly compared to effective ab-initio calculations and used to constrain nuclear contact terms.

We will use 25–40 μA of the 11 GeV beam in Hall-C, detecting the scattered electrons in the SHMS in coincidence with the knocked out protons in the HMS. We request 7 days of beam-time to significantly improve our quantitative understanding of nucleon pairing in nuclei.

I. INTRODUCTION AND MOTIVATION

A. Short Range Correlated NN Pairs in Nuclei

The mean field approximation describes bulk properties of nuclei—shell structure, excitation energies, spins and parities—remarkably well; however, only about 70% of nucleons occupy mean field orbitals [1, 2]. Describing the dynamics of the remaining long- and short-range correlated nucleons is a major challenge facing nuclear physics today.

The Jefferson Lab 6 GeV program made tremendous progress in understanding the Short-Range Correlated (SRC) nucleons. Results from inclusive (e, e') measurements at $x = Q^2/2m\nu > 1$ (see Section II B for variable definitions) indicate that all nuclei have remarkably similar nucleon momentum distributions for $k > 275$ MeV/$c \approx k_F$ [3–5], and that in medium and heavy nuclei about 20–25% of nucleons have momenta greater than the typical Fermi momentum [4, 5].

Exclusive $(e, e'pN)$ measurements show that in the symmetric ^{4}He and ^{12}C nuclei, almost every proton with momentum $300 < k < 600$ MeV/c has a correlated partner nucleon, with neutron-proton (np) pairs outnumbering proton-proton (pp) and, by inference, neutron-neutron (nn) pairs by a factor of ~ 20 [6–8]. This preference for np-SRCs is understood to arise from the dominance of the tensor part of the NN interaction at short distances [9–11]. In asymmetric, heavy nuclei, with more neutrons than protons, high-momentum neutrons still disproportionately belong to np-SRC pairs [12]. The observed np-SRC dominance in heavy nuclei is a non-trivial result since, in these heavy nuclei, nucleons from different shells can create $l \neq 0$ pp and nn pairs with non-zero spin, which are also sensitive to the tensor part of the NN-interaction, thereby diminishing the np dominance. Two of these results were published in *Science* [6, 12].

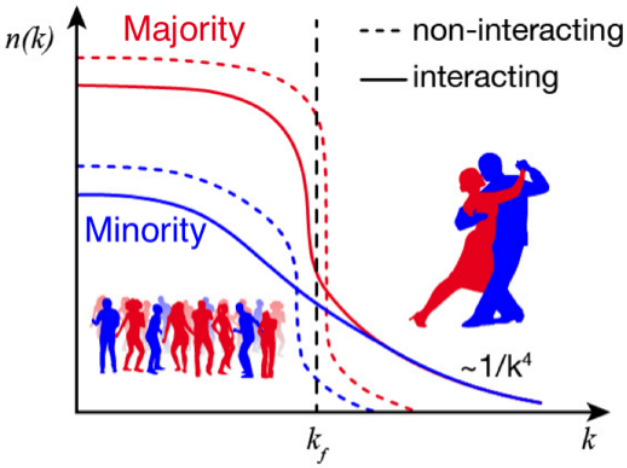

FIG. 1: A schematic representation of the main characteristics of the momentum distribution, $n(k)$, of asymmetric nuclei. The dashed lines show the standard non-interacting Fermi system while the solid lines show the effect of including a short-range interaction between different Fermions which creates a high-momentum ($k > k_F$) tail. This is analogous to a dance party with a majority of girls, where the dominance of heterogenous interactions will make the average boy dance more than the average girl, and hence the boys will have larger average momentum [12].

The observed np-SRC pair dominance also implies that in heavy neutron-rich nuclei the high-momentum tail contains the same amount of neutrons and protons, leaving the excess neutrons to occupy low-momentum states (see Fig. 1). This leads to a possible inversion of kinetic energy sharing between protons and neutrons where protons (i.e. the minority) have larger average kinetic energy compared to neutrons (i.e. the majority).

Since nearly all high-momentum protons in nuclei are part of NN-SRC pairs, we used the measured number of high-momentum protons to infer the number of pp and pn-SRC pairs in a given nucleus [12].

A recent CLAS6 data mining analysis by Meytal Duer (currently undergoing CLAS analysis review) extracted the relative number of low-p_{miss} and high-p_{miss} protons and neutrons in C, Al, Fe, and Pb by measuring the $A(e, e'p)$ / $A(e, e'n)$ reduced cross-section ratio (experimental cross-section relative to the free electron-proton to electron-neutron cross-section ratio). The results, shown in Fig. 2, indicate that while the relative number of mean-field neutrons to protons grows like N/Z, the relative number of high-momentum (SRC) neutrons to protons is constant, irrespective

of the nuclear neutron excess. The lack of dependence on neutron excess is consistent with the notion that NN-SRC pairs are predominantly np in character.

The attribution of the above result to np-dominance relies on the assumption that the experiment is measuring nucleons from SRC pairs. If instead, the measurement were dominated by Final State Interactions (FSIs) or other reaction mechanisms, it would also be possible to observe a flat neutron-to-proton ratio. As a test to reject this scenario, Fig. 3 shows, for protons and neutrons separately, the relative fraction of high-momentum nucleons in various asymmetric nuclei relative to the symmetric nucleus ^{12}C. This is defined as the double cross-section ratio of high-momentum to mean-field nucleons in nucleus A relative to ^{12}C (i.e. $[A(e,e'p)_{high-P}/A(e,e'p)_{mean-field}]/[^{12}C(e,e'p)_{high-P}/^{12}C(e,e'p)_{mean-field}]$). While the fraction of correlated protons increases with neutron excess, the fraction of correlated neutrons shows no rise and, in fact, is less than unity in ^{208}Pb. As these measurements were made at large momentum transfers ($\langle Q^2 \rangle \sim 2$ GeV^2)—where the rescattering cross sections for protons and neutrons are similar—this difference between the two can not be simply explained by FSIs.

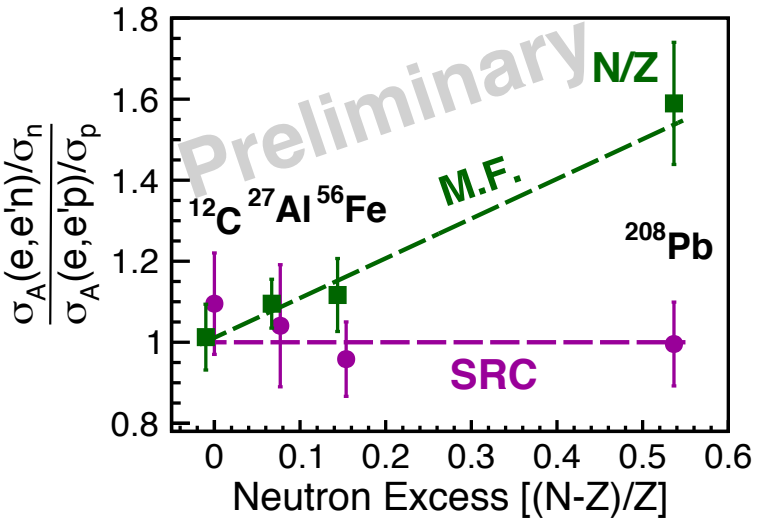

FIG. 2: The $A(e,e'p)/A(e,e'n)$ reduced cross-section ratio for low-p_{miss} (mean-field) [green squares] and high-p_{miss} [SRC] (purple circles) events plotted versus neutron excess. The dashed lines are simple model predictions for the N/Z neutron excess-dependence of the Mean-Field nucleons and the independence of neutron excess of the SRC nucleons.

Fig 3 also shows a comparison with a simple phenomenological np-SRC dominance model [12]. The model used one of several mean-field momentum distributions for $k \leq k_F$ and a scaled deuteron momentum distribution for $k \geq k_F$. The deuteron scaling for the proton and neutron distribution ensures the same number of high-momentum protons and neutrons and a total number of correlated nucleons based on the measured (e,e') cross sections [3–5], see Ref. [12] for details. The agreement of the model with the data is impressive. This model also predicts that the ratio of the neutron to proton average kinetic energies decreases with neutron excess such that protons move faster than neutrons in neutron-rich nuclei (see Fig. 4).

Thus, the preliminary CLAS results provide direct affirmative evidence for the dominance of np pairs in heavy nuclei with mininal assumptions. It also supports the ability to calculate FSI in SRC pairs breakup kinematics (used in this proposal) using Glauber approximation, and the validity of our proposed technique: using the ratio of high-p_{miss} to low-p_{miss} $(e,e'p)$ cross-section ratios to determine the relative fraction of protons belonging to SRC in the different nuclei.

The new experimental results on the pairing fractions for protons and neutrons in different nuclei, from the above CLAS analysis and others, can interface with theory in several concrete ways. Firstly, there have been tremendous recent advances in ab initio calculations of one- and two-body nucleon distributions in light nuclei. Monte-Carlo techniques can now reach up to ^{40}Ca [13, 14], while coupled-cluster techniques have a predictive scope that extends to even heavier nuclei [15–17], and the more-effective density-function theory can make predictions in some of the heaviest nuclei [18]. Recent progress using contact formalism [19], convolution approaches [20, 21], and correlation

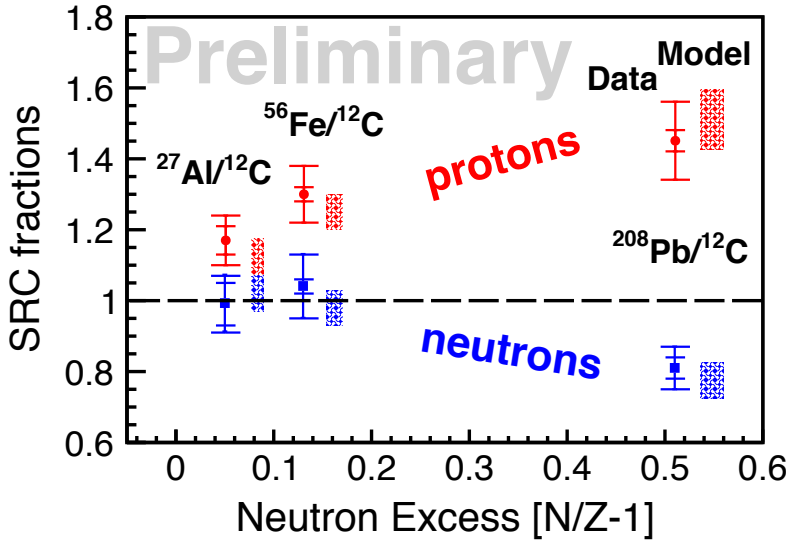

FIG. 3: Red points: The double ratio of the number of $(e, e'p)$ high-p_{miss} (SRC) proton events to low-p_{miss} (mean field) proton events for nucleus A relative to Carbon plotted versus the neutron excess of nucleus A. Red boxes: the prediction of the phenomenological np-dominance model. Blue points and boxes: the same for neutrons.

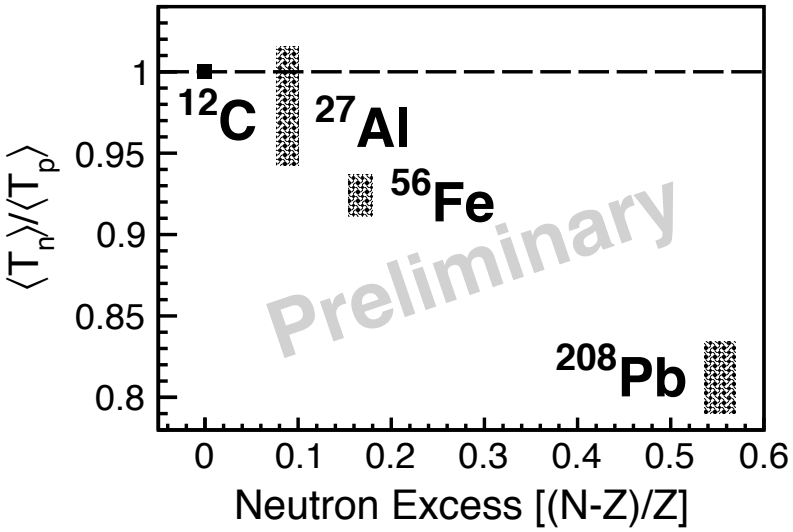

FIG. 4: The ratio of the neutron to proton average kinetic energy, as obtained from the np-SRC dominance model, as a function of the neutron excess. This indicates that protons move faster than neutrons in neutron rich nuclei.

operators [22] has demonstrated that the high-momentum (or, alternately, short-distance) parts of the many-body nuclear wave function effectively factorize into a contact parameter, which depends on the nuclear many-body dynamics and the spin and isospin of the short-range pairs being considered, and a universal two-body distribution, which does not depend on the nucleus being considered. The contact terms relate directly to both the pairing fractions for protons and neutrons, and to ab-initio calculations of ground state one and two body densities, providing a bridge between the measured cross-section and theoretical calculations [19].

B. Implications of kinetic energy sharing in asymmetric nuclei

The *np*-dominance of SRC pairs and the resulting inversion of the kinetic energy sharing in heavy neutron-rich nuclei have potentially wide-ranging implications in astro, nuclear and particle physics. These include the determination of the density dependence of the nuclear symmetry-energy up to supra-nuclear densities [23–28], analysis of neutrino-nucleus scattering data for determining the nature of the electro-weak interaction [29, 30], the quark structure of bound nucleons through the EMC effect [31, 32], the isospin dependence of the EMC effect as a cause of the standard-model NuTeV anomaly [31, 33–36], double-beta decay matrix elements [37, 38], neutron star equation of state and cooling rates [39], etc.

Following the PAC-44 report, we focus below on a few quantitative examples for the implications of the SRC high-momentum tail's existence and of the inversion of the kinetic energy sharing in nuclei.

1. *Symmetry energy*

Detailed measurements of the mass number and isospin dependences of SRCs can improve calculations of the properties of neutron stars. Many of the large-scale properties of neutron stars—their equation of state, their cooling rate, the behavior of their core-crust transition, to name a few—are largely governed by the nuclear symmetry energy, a parameter that describes how the energy per nucleon in nuclear matter changes as a function of the proton fraction. While the symmetry energy is well constrained at the nuclear saturation density [27], its density dependence is not. This density dependence is a crucial input to calculations of neutron star properties. While it has long been known that low energy pairing effects have a significant impact on this density dependence (see Ref. [40]), recent works show that SRCs also play a role.

Recent calculations by Bao-Jun Cai and Bao-An Li show the effect of SRCs on the density-dependence of the symmetry energy within a modified Gogny-Hartree-Fock energy density functional approach [41]. The results are shown in Fig. 5. In this figure, the symmetry energy is shown as a function of the density with and without the high momentum tail produced by $2N$-SRCs. With the inclusion of an SRC model, there are large changes in predictions for the proton fraction in neutron stars as well as in the core-crust transition density and pressure in neutron stars [41]. A similar study found that the addition of a model for *np*-SRCs significantly improves nuclear incompressibility isospin-dependence calculations, bringing the results closer to experimentaly extracted values [42].

Since SRCs can make dramatic changes to calculations of neutron stars, better quantitative knowledge of the proton and neutron pairing probabilities, as functions of mass and proton-neutron asymmetry, can immediately offer better constraints of various aspects of neutron star properties.

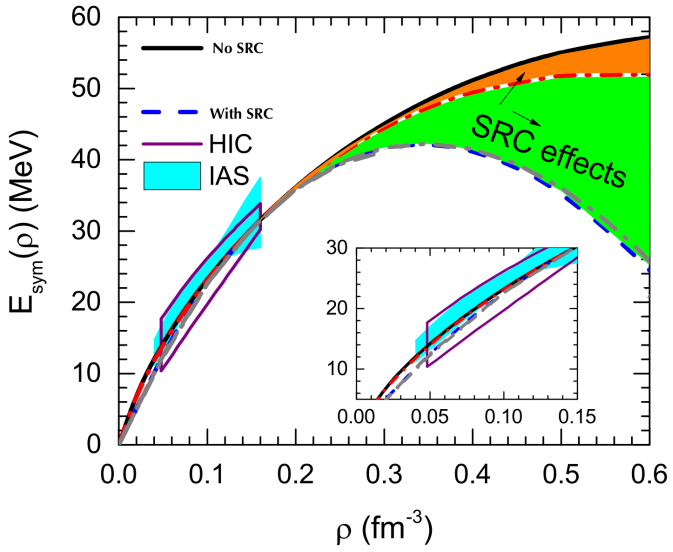

FIG. 5: Density dependence of nuclear symmetry energy $E_{sim}(\rho)$ calculated with and without the SRC high-momentum tail. Constraints on the symmetry energy from analyzing heavy-ion collisions (HICs) and isobaric analog states (IASs) are also shown for comparison. The figure was adapted from [41] and modified by us for clarity.

2. Neutrino-nucleus scattering

A better understanding of SRCs in asymmetric nuclei and constraining the correlated region of the distorted nuclear spectral function can significantly improve the precision attained by the next generation of neutrino oscillation experiments. Neutrino oscillation analyses rely on models of the neutrino-nucleus interaction, but until recently, most analysis used a simplified relativistic Fermi gas model to describe the nucleus, a model which ignores SRCs. Recent calculations of the effects of SRCs on neutrino-nucleus interactions show their influence on one- and two-nucleon knockout processes, affecting the expected quasi-elastic signal [43]. This is also seen experimentaly, where high-precision measurements of charged current quasi-elastic neutrino-nucleus scattering cross-sections [29, 30] show the need to include the effects of NN-SRC pairs in both their reaction model and detector response. SRCs are expected to be a crucial ingredient in modeling neutrino and anti-neutrino interactions with asymmetric nuclei, necessary for facilitating the precision requirements of next generation neutrino experiments [44].

A quantitative example for the effects of correlations on neutrino-oscillation analyses is presented in Figure 6, which shows a calculation of the expected $1\mu 1p$ events rate distribution in the MicroBooNE experiment for muon and electron neutrinos with and without SRCs. This calculation is part of an ongoing estimation of the expected 'no oscillation' prediction, to be used for sterile neutrino searches. The energy range shown is the one used to search for low energy oscillations, where the predecessor MiniBooNE experiment observed an unexplained excess of neutrino-interaction events. The calculation was done using the GENIE Monte Carlo event generator—commonly used by neutrino experiments at Fermilab and around the world—taking into account the MicroBooNE incident electron and muon neutrino energy distribution, detection thresholds, event containments cuts, and $1\mu - 1p$ event selection criteria. The 3 lines correspond to different models used to describe the ground state momentum distribution of nucleons. These include the commonly used Relativistic Fermi-Gas (RFG) model, the recently added Local Fermi-Gas (LFG) model, and a new Correlated Fermi-Gas (CFG) model which includes high-momentum np-SRC pairs. As seen in the figure, the addition of correlations can alter the count rate by 10–20% and affect the measured electron-neutrino to muon-neutrino rates. The later serves as a reduced systematic uncertainty test for such high-precision measurements. It should be noted that Ref [45] found similar effects in other oscillation analyses.

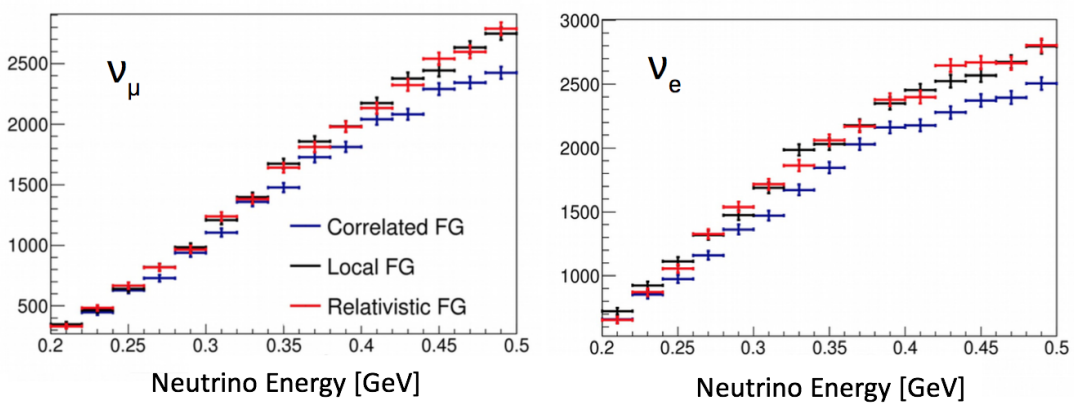

FIG. 6: Expected event rate distribution for the MicroBooNE experiment calculated with the GENIE Monte Carlo event generator using three different models for the nuclear momentum distribution. The difference between the Relativistic and Local Fermi-Gas calculations (Black and Red) and the Correlated Fermi-Gas reflects the effect of SRCs. See text for details.

The proposed experiment will help us understand which nucleons form SRC pairs, which, in turn, will improve our understanding of neutrino-nucleus interactions. In this way, these proposed measurements will complement experiment E12-14-012, which just completed a measurement of $\mathrm{Ar}(e,e'p)$ and $\mathrm{Ti}(e,e'p)$ cross-sections to extract the mean-field spectral function (i.e., the single-nucleon properties and spectroscopic factors) of ^{40}Ar and ^{48}Ti. It will also complement the "Electrons for Neutrinos" proposal to this PAC by measuring the $\mathrm{Ar}(e,e'p)$ cross-section at SRC kinematics as a function of missing momentum and missing energy with far better precision than is possible with CLAS12. By comparing these data to generator calculations, we will be able to constrain the high momentum region of the distorted spectral function that is used as input in neutrino interaction event generators.

3. The EMC effect and the NuTeV anomaly

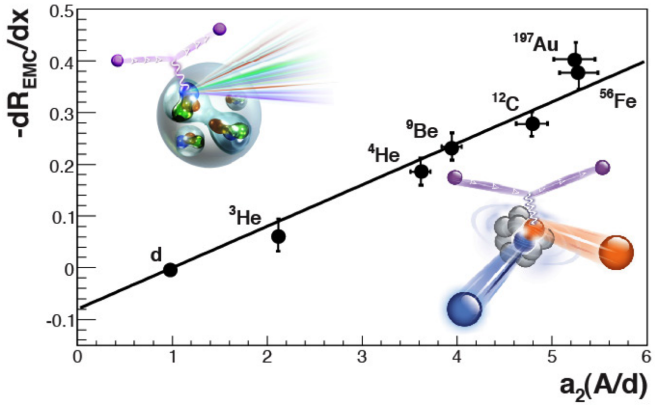

FIG. 7: The strength of the EMC effect plotted vs. the relative probability for a nucleon to belong to an SRC pair for a variety of nuclei. See Refs. [31, 32, 46] for details.

The deep inelastic scattering cross section for scattering from bound nucleons differs from that of free nucleons. This phenomenon, first discovered 30 years ago, is known as the EMC effect, and its origin is still not fully understood [46–51]. The EMC effect implies modification of bound nucleon structure [46, 51] and its size is found to linearly correlate with the number of SRC (high momentum) pairs in nuclei (see Fig. 7) [31, 32, 52]. This supports theoretical models relating the EMC effect to high momentum (i.e., large virtuality) nucleons in the nucleus. The latter are predominantly part of NN-SRC pairs. Two 12-GeV JLab experiments will measure deep inelastic scattering (DIS) off one nucleon in the deuteron by detecting (tagging) high-momentum backward-angle spectator protons [53] or neutrons [54]. By measuring the nucleon-momentum dependence on bound nucleon structure functions, these experiments will determine whether the EMC effect is due to a small modification of the large number of mean-field nucleons or a large modification of the smaller number of SRC nucleons.

Calculations of the EMC effect generally have two ingridients: (1) conventional nuclear physics effects and (2) an in-medium nucleon modification model. As explained below, NN-SRCs affect both parts of the calculation.

The calculations of conventional nuclear physics effects are traditionaly viewed as a 'base line' to which the data should be compared in order to estimate the size of more exotic effects, i.e., bound nucleon modification, still required to explain the data. Fig. 8 shows the measured EMC ratio for ^{56}Fe compared to two conventional nuclear physics effects (including Fermi-motion, binding etc., but no medium modification), including and excluding effects of SRCs. It is clear from the figure that the effects of SRCs are large and enter into the calculation via an increase in the average nucleon kinetic energy used in a standard convolution formalism [55–59].

When examining the possible isospin dependence of the EMC effect, the effects of SRC are more delicate, and special care should be given to properly account for the relative correlation probabilities of protons and neutrons. As the high-x proton structure function is larger than that of the neutron, differences between the proton and neutron average kinetic energies change the expected effect of conventional nuclear physics effects. Figure 8 also shows an example for the possible effect of np-SRCs on the ^{48}Ca/^{40}Ca EMC ratio that will be measured as part of approved experiment E12-10-008. The calculation is done using estimates based on Ref. [12], however detailed knowledge of the SRC pairing probabilities is needed to fully constrain it. As seen in Fig. 8, the potential effects of np-SRC are large and should be properly accounted for in order to interpret any possible deviation of the measured EMC ratio from unity as evidence for isospin dependence. The proposed measurement will constrain the relative proton and neutron pairing probabilities and hence the nuclear base line effects.

Theoretical calculations show that such an isospin dependent EMC effect in neutron-rich nuclei, and in particular iron, could explain the NuTeV anomaly [36]. The latter is a three standard deviation difference from the Standard Model prediction in the measurement of the electroweak-mixing (Weinberg) angle using neutrino scattering from iron [35].

One original model employed a mean-field model to explain the possible existence of such an isospin dependent result [60]. The EMC-SRC correlation implies that the EMC nucleon modification instead is dominated by high momentum nucleons. One attractive model for this [46] describes the nucleon as a superposition of a normal nucleon with a small admixture of a "Point Like Configuration" (PLC), which experiences much less nuclear attraction than

the normal nucleon. Nucleons that fluctuate into a high-momentum short-range pair will briefly have much greater kinetic energy, and hence much greater potential energy. This increased potential energy will suppress the PLC amplitude, modifying the quark distribution in the nucleon.

Because nucleon modification is very sensitive to nucleon kinetic energy in this model, it will be sensitive to the details of pairing in asymmetric nuclei. Specifically, if protons have higher average kinetic energy than neutrons in neutron rich nuclei, then this would provide for an isospin dependent EMC effect which could quantitatively explain the NuTeV anomaly.

By studying the nuclear asymmetry dependence of the number of correlated protons and neutrons separately, our proposed measurement will provide input and constraints to calculations of both the conventional nuclear physics effects and the structure function modifications for the EMC effect in general and the NuTeV anomaly specifically.

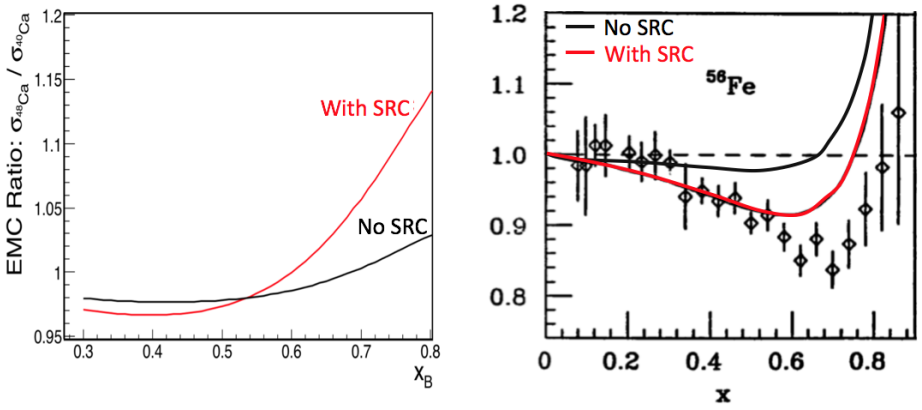

FIG. 8: Baseline calculations (Fermi motion and binding, no nucleon modification) for the ^{56}Fe/d EMC measurement (right) and the ^{48}Ca/^{40}Ca EMC ratio (left), with (red) and without (black) *np*-SRC pairs.

II. SHORT RANGE NUCLEON PAIRING

We propose to measure the relative proportion of high-momentum protons in d, ^{4}He, ^{9}Be, ^{10,11}B, ^{12}C, ^{28}Si, ^{40}Ar, ^{40,48}Ca, ^{48}Ti and ^{54}Fe to test short range pairing mechanisms.

Deuterium, as the simplest nuclear system, will serve as a benchmark. d, ^{4}He, ^{10}B, ^{12}C, ^{28}Si and ^{40}Ca will be used to establish the nuclear mass dependence in symmetric nuclei and constrain nuclear transparency corrections. The rest will be used to study the effect of isospin asymmetry, comparing ^{40}Ar vs. ^{40}Ca, ^{40}Ca vs. ^{48}Ca, ^{48}Ca vs. ^{48}Ti etc.

The ^{40}Ca-^{48}Ca-^{54}Fe triplet is of particular interest. ^{40}Ca and ^{48}Ca are both doubly magic nuclei. ^{40}Ca has filled proton and neutron in the $1s, 1p$, and $2s/1d$ shells. ^{48}Ca has, in addition, eight more neutrons in the $1f_{7/2}$ outer shell. The exact way in which these extra $1f_{7/2}$ neutrons form SRC pairs with the 40 nucleons in the inner core is non-trivial.

E08-014 measured the per-nucleon ratio of (e, e') cross sections for ^{48}Ca to ^{40}Ca at $1.25 \leq Q^2 \leq 2$ GeV^2 [61]. The preliminary results are shown in Fig. 9, and suggest a cross section ratio of 0.97. Using the formalism described below to compare with calculations, we find this ratio to be generally consistent with but slightly smaller than coupled-cluster calculations using the N^2LO_{sat} interaction (also described below). However, the quantitative interpretation of this measurement in terms of pair isospin structure is non-trivial. Simple combinatorical counting considering either only np pairs or all possible pairs both give very similar predictions. This is primarily because the (e, e') reaction is sensitive to both protons and neutrons, preventing a detailed understanding of the pairing mechanisms. As will be discussed below, the addition of $(e, e'p)$ measurements will allow the separation of the different pairing probabilities in protons and neutrons, facilitating a detailed comparison to calculations.

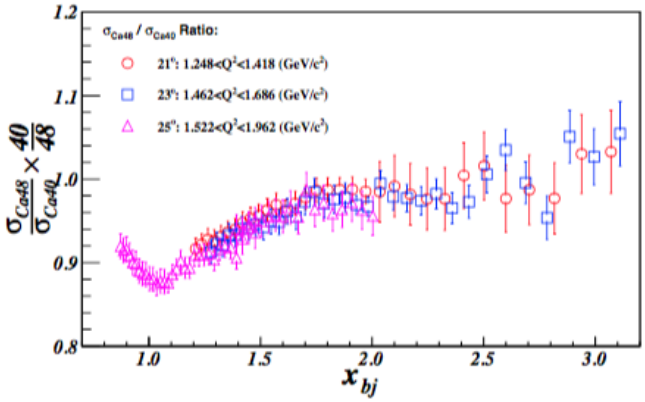

FIG. 9: The per-nucleon (e, e') cross section ratio of ^{48}Ca to ^{40}Ca. The ratio in the scaling region ($1.7 < x < 2$ for $Q^2 \approx 1.3$ GeV^2 and $1.5 < x < 2$ for $Q^2 \approx 2$ GeV^2) is about 0.97. The figure is taken from [61].

By extracting the relative number of high-momentum protons in ^{40}Ca and ^{48}Ca nuclei, we can directly measure the extra number of cross-shell np pairs caused by adding eight $1f_{7/2}$ neutrons. Similarly, by adding six $1f_{7/2}$ protons to ^{48}Ca, we get ^{54}Fe. These extra protons can pair with any of the 40 nucleons in the inner shells or with the eight neutrons in the $1f_{7/2}$ shell. Thus, measuring the difference between ^{40}Ca and ^{48}Ca will teach us about the pairing of protons and neutrons from different shells and measuring the difference between ^{48}Ca and ^{54}Fe will teach us about the pairing of protons and neutrons from both different shells and the same shell.

As ab-initio calculations for light nuclei are readily available using various NN interaction models and calculation schemes, we will also study the effect of single proton and neutron addition to light nuclei by measuring the ^{9}Be-^{10}B-^{11}B chain and compare all nuclei to Deuterium as the basic np systems.

Based on the new asymmetric nuclei measurements shown in Fig. 2, we expect that the number of protons and neutrons in all asymmetric nuclei to be the same. Fig. 10 shows the ratio of the neutron-to-proton momentum distribution in ^{48}Ca, as obtained from a recent state-of-the-art ab-initio calculations using the Coupled-Clusters (CC) method and the N2LO$_{SAT}$ NN interaction [17]. For momentum above approximately 400 MeV/c, $n^p_{^{48}\mathrm{Ca}}(k)/n^p_{^{40}\mathrm{Ca}}(k)$ is greater than 1.2. This calculation therefore stands in contrast with the phenomenological expectation based on the measurements shown in Fig. 2.

Medium mass nuclei calculations using other NN interactions just became available for symmetric nuclei (ranging up to ^{40}Ca) [13], but are not yet available for asymmetric nuclei. Fig. 11 shows a comparison of ^{40}Ca momentum distributions obtained from a recent Variational Monte-Carlo (VMC) calculation using the AV18+UIX NN interaction

and CC using N2LO$_{SAT}$ NN interaction. As seen in the figure, due to the soft nature of the N2LO$_{SAT}$ NN interaction and the lower cutoff used in the calculation, the resulting momentum distributions differ significantly at high-momentum. While calculations based on the AV18+UIX interactions are not yet available for medium mass asymmetric nuclei, they are expected to become available soon [62].

For light nuclei, Fig. 12 shows VMC calculations of the ratio of the average proton momentum distribution in ^{10}B relative to ^{9}Be (left plot) and in ^{11}B relative to ^{10}B (right plot). These calculations show that the addition of a neutron to ^{10}B leads to more correlated protons, consistent with the np-SRC domiance described above. Comparing ^{10}B and ^{9}Be (same number of neutrons, one proton difference) we see that the average proton in ^{9}Be is more correlated than in ^{10}B. These calculated quantities can be directly compared to the measured differential cross-sections, after corrections for FSI. An alternative is to compare integrals over the calculated momentum distirbutions (e.g. shaded regions in Fig. 10) that are sensitive to the pairing dynamics but less sensitive to detailed FSI corrections.

These different predictions can be tested by the proposed ^{40}Ca and ^{48}Ca$(e,e'p)$ measurements combined with the existing ^{40}Ca and ^{48}Ca(e,e') data, see details below.

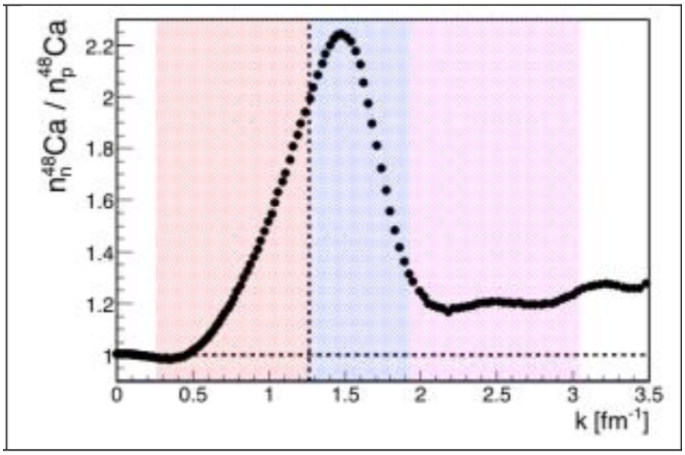

FIG. 10: The ratio of neutron to proton single-particle momentum distributions in ^{48}Ca as calculated using the CC method and the N2LO$_{SAT}$ NN interaction [17]. This can be extracted from the measured cross-section ratios after FSI corrections and can also be compared to integrals over the shaded regions that have reduced sensitivity to detailed FSI corrections.

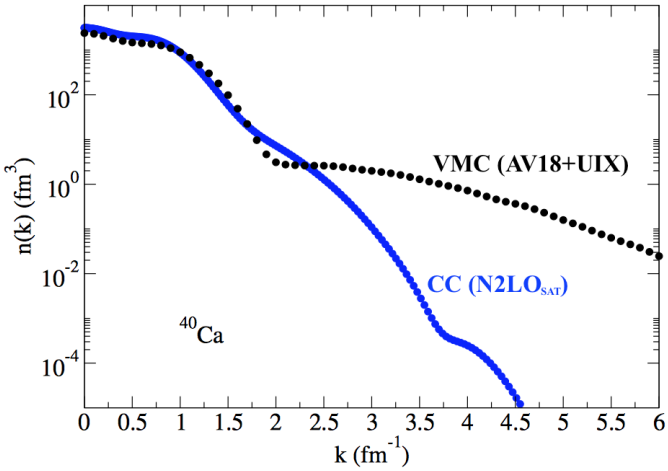

FIG. 11: The single-particle momentum distributions in ^{40}Ca as calculated using the CC method and the N2LO$_{SAT}$ NN interaction [17] and the VMC method and the AV18+UIX interaction [13].

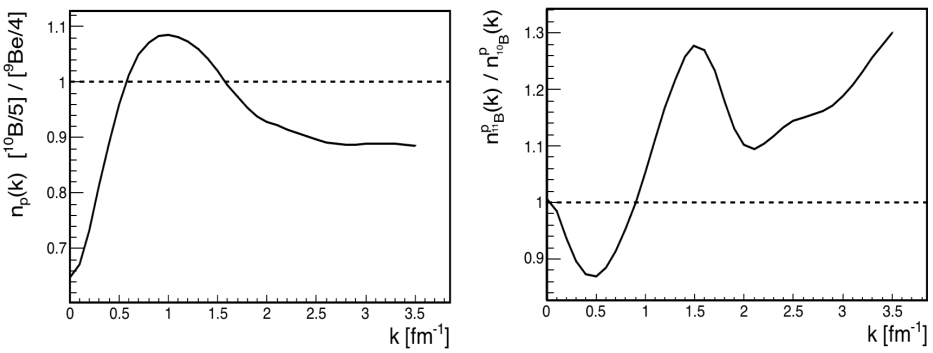

FIG. 12: Ratios of proton momentum distributions [^{10}B / ^{9}Be] (left plot) and [^{10}B / ^{11}B] (right plot) calculated using the VMC method and the AV18+UIX interaction. See text for details.

A. Contact formalism

Here we present a simplified version of the Contact formalism that can be used to relate the (e,e') and $(e,e'p)$ cross-section ratios to ab-initio calculations of one and two body momentum densities such as the once presented above. The formalism is given for ^{40,48}Ca but can be applied to all nuclei.

We begin by defining the fraction of correlated nucleons in a nucleus (A) as χ^{N-A}_{SRC}, where $N = n,p$ stands for protons or neutrons. Using these fractions, the number of SRC nucleons in ^{40}Ca is given by:

$$\#\text{ SRC nucleon} = 20\cdot\chi^{p-40Ca}_{SRC} + 20\cdot\chi^{n-40Ca}_{SRC} = 40\cdot\chi^{N-40Ca}_{SRC} \tag{1}$$

Similarly, for ^{48}Ca:

$$\#\text{ SRC pairs} = 20\cdot\chi^{p-48Ca}_{SRC} + 28\cdot\chi^{n-48Ca}_{SRC}. \tag{2}$$

The inclusive (e,e') cross-section ratio,

$$R^{48/40}_{(e,e')} \equiv \left[\frac{\sigma_{^{48}\mathrm{Ca}(e,e')}}{\sigma_{^{40}\mathrm{Ca}(e,e')}}\right]_{x_B\gtrsim 1.4}, \tag{3}$$

is sensitive to both correlated protons and neutrons and can be expressed as:

$$\frac{\sigma_p\cdot 20\cdot\chi^{p-48Ca}_{SRC} + \sigma_n\cdot 28\cdot\chi^{n-48Ca}_{SRC}}{[\sigma_p+\sigma_n]\cdot 20\cdot\chi^{N-40Ca}_{SRC}} = \frac{\chi^{p-48Ca}_{SRC} + \frac{\sigma_n}{\sigma_p}\cdot 1.4\cdot\chi^{n-48Ca}_{SRC}}{\left[1+\frac{\sigma_n}{\sigma_p}\right]\cdot 2\cdot\chi^{N-40Ca}_{SRC}} = R^{48/40}_{(e,e')}, \tag{4}$$

where σ_p (σ_n) are the electron - off-shell proton (neutron) cross-sections.

Similarly, the measured $(e,e'p)$ cross-section ratio,

$$R^{48/40}_{(e,e'p)} \equiv \left[\frac{\sigma_{^{48}\mathrm{Ca}(e,e'p)}}{\sigma_{^{40}\mathrm{Ca}(e,e'p)}}\right]_{p_{miss}>300\text{ MeV/c}} \tag{5}$$

can be expressed as:

$$T_{48/40}\cdot\frac{20\cdot\sigma_p\cdot\chi^{p-48Ca}_{SRC}}{20\cdot\sigma_p\cdot\chi^{N-40Ca}_{SRC}} = T_{48/40}\cdot\frac{\chi^{p-48Ca}_{SRC}}{\chi^{N-40Ca}_{SRC}} = R^{48/40}_{(e,e'p)}, \tag{6}$$

where $T_{48/40}$ is the transparency ratio for proton knockout off ^{48}Ca relative to ^{40}Ca.

Combining Eq. 4 and 6 one can extract the ratio of the fraction of correlated neutrons to correlated protons in ^{48}Ca, $\chi^{n-48Ca}_{SRC}/\chi^{p-48Ca}_{SRC}$, in terms of the measured cross-section ratios:

$$\frac{\chi^{n-48Ca}_{SRC}}{\chi^{p-48Ca}_{SRC}} = \frac{1}{1.4}\frac{\sigma_p}{\sigma_n}\cdot\left[2\cdot\left(1+\frac{\sigma_n}{\sigma_p}\right)\cdot T_{48/40}\cdot\frac{R^{48/40}_{(e,e')}}{R^{48/40}_{(e,e'p)}} - 1\right] \tag{7}$$

Both the ratios of Eq. 6 and 7 can be compared to ab-initio calculations. As stated above, we expect that the ratio in Eq. 7 (after N/Z normalization) to be equal to unity, in contrast to the coupled-cluster prediction shown in Fig. 10.

B. Formalism for A$(e, e'p)$ measurement

The cross section for electron-induced proton knockout from nuclei $A(e, e'p)$ can be written (assuming factorization) as:

$$\frac{d^6\sigma}{d\nu dE_{miss} d\Omega_e d\Omega_p} = K\sigma_{ep} S^D(E_{miss}, p_{miss})$$

where σ_{ep} is the cross section for scattering an electron from a bound proton. The missing energy and missing momentum are

$$E_{miss} = \nu - T_p - T_{A-1} \quad (8)$$
$$\vec{p}_{miss} = \vec{q} - \vec{p}_p \quad (9)$$

where T_p and T_{A-1} are the kinetic energies of the outgoing proton and residual nucleus, the momentum transfer $\vec{q} = \vec{p}_e - \vec{p}'_e$, $S^D(E_{miss}, p_{miss})$ is the distorted spectral function and the kinematical factor K

$$K = \frac{E_p p_p}{(2\pi)^3}.$$

In the absence of final state interactions (FSI), S is the probability to find a nucleon in the nucleus with separation energy E_{miss} and momentum p_{miss} [63]. The energy transfer $\nu = E - E'$, E and E' are the initial and scattered electron energies, $\vec{p}_e$ and $\vec{p}'_e$ are the initial and scattered electron momenta, $\vec{p}_p$ is the outgoing proton momentum, and Ω_e and Ω_p are the electron and proton solid angles respectively. The angle between the recoil momentum ($\vec{p}_{recoil} = \vec{p}_{miss}$) and $\vec{q}$ is called θ_{rq}. We will restrict θ_{rq} to minimize final state interactions (see Section II C for details).

We plan to extract the distorted spectral function, as a function of missing momentum and energy, from the measured cross sections:

$$S^D(E_{miss}, p_{miss}) = \left(\frac{1}{K\sigma_{ep}}\right) \frac{d^6\sigma}{d\nu dE_{miss} d\Omega_e d\Omega_p}, \quad (10)$$

and then correct it for the effects of FSI.

For each nucleus we plan to measure at one low-p_{miss} kinematics and one high-p_{miss} kinematics. We will correct the distorted spectral function for FSI. For each value of missing momentum we will only detect protons covering a fraction $f(p_{miss})$ of the 4π solid angle available to $\vec{p}_{miss}$. We will further correct our measurement by $1/f$ to account for this. We will then integrate the corrected distorted spectral functions over missing energy and missing momentum. The relative amount of high-momentum protons in each nucleus will equal the ratio of the integrated distorted spectral functions at high-p_{miss} and low-p_{miss}.

The double ratio of the integrated distorted spectral functions at high-p_{miss} and low-p_{miss} for different nuclei should correspond to the ratios of ab initio one-body momentum densities at high momentum.

The correction, $1/f$, for the undetected protons is mostly geometrical. It is easy to calculate and will also cancel in the double ratio of high-p_{miss} and low-p_{miss} for different nuclei.

There are a number of uncertainties in the extraction of the distorted spectral function, including the validity of factorization, the off-shell extrapolation of the electron-proton cross section, and the effects of FSI. Over the limited acceptance of the spectrometers, factorization should be accurate to about 10% and the effects of factorization should cancel almost completely when calculating cross section ratios. Similarly, while there are several different off-shell prescriptions for the electron-proton cross section [64], the effects of these will also cancel when calculating ratios at similar p_{miss}. The effect of FSI is discussed in section II C.

C. Final State Interactions

We want to extract absolute and reduced cross sections for the $A(e, e'p)$ reaction for a variety of nuclei, which will allow us to extract the following ratios:

- ratios of high to low momentum protons in each of the measured nuclei,
- ratios of high-momentum protons in heavier nuclei to deuterium and to the closest symmetric nucleus,
- double ratios of high to low momentum protons in heavier nuclei and to the closest symmetric nucleus.

We will need to correct each of these ratios for the effects of final state interactions (FSI).

There are two general effects from rescattering of the outgoing proton: a shift in momentum due to the real part of the proton-nucleus potential, and rescattering of the proton that changes its momentum and potentially knocks out a second nucleon. Loss of protons from a particular kinematic bin can be calculated accurately in the Glauber approximation for high momentum protons. Rescattering of protons into a particular kinematic bin is harder to calculate.

We will measure the $(e, e'p)$ reaction at small angles between the momentum transfer and the recoil momentum, $\theta_{rq} \leq 40°$, to significantly reduce contributions from nucleon rescattering.

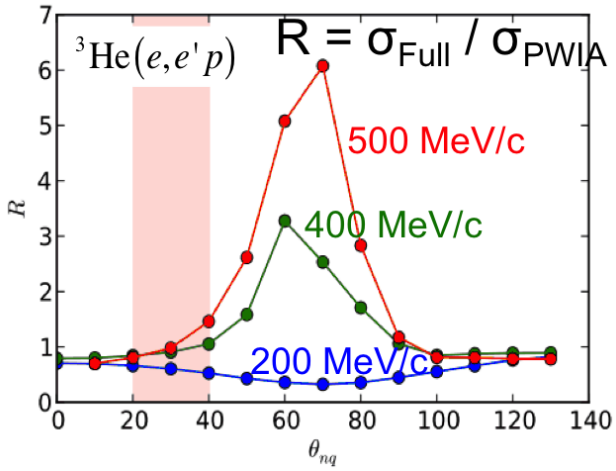

FIG. 13: The calculated ^{3}He$(e, e'p)$ ratio of the cross section which includes rescattering of the struck nucleon (FSI) to the PWIA cross section for $p_{miss} = 0.2$ (blue), 0.4 (green), and 0.5 (red) GeV/c as a function of θ_{rq}, the angle between the recoil momentum and $\vec{q}$ in the laboratory frame [65].

This rescattering of protons *into* a particular kinematic bin is maximum at perpendicular kinematics, where the angle between the recoil momentum and the momentum transfer, $\theta_{rq} \approx 70°$. This happens because most collisions between high-momentum protons and other nucleons in the nucleus deflect the high-momentum only slightly, kicking the struck nucleon out at about 70° (non-relativistically it would be about 90°). This can be seen clearly in calculations of the data of [66], where the cross section at $p_{miss} > 250$ MeV/c and $E_{miss} \approx p^2_{miss}/2m$ is due almost entirely to rescattering. Calculations by Sargsian [65] for ^{3}He$(e, e'p)$ show very large contributions due to proton rescattering peaked at $\theta_{rq} \approx 70°$. In order to avoid these regions where rescattering is much larger than the SRC signal, we will choose $\theta_{rq} \leq 40°$.

We will calculate the rescattering of protons *out* of our kinematic bins using the Glauber approximation. Glauber calculations have been shown to reproduce nucleon transparency measurements in nuclei [67]. In addition, since we are primarily interested in the relative proportions of high- and low-initial-momentum protons in the different nuclei, we are primarily sensitive to the *difference* in the transparency.

We consider here, for example, ^{40}Ca and ^{54}Fe(same considerations hold for the other nuclei). The measured transparency in ^{56}Fe at $Q^2 = 3.3$ GeV^2 is $T = 0.4$ [68]. The calculated transparency for knocked-out protons at $Q^2 = 2.4$ GeV^2 and $50 \leq p_{miss} \leq 150$ MeV/c (i.e., for kinematics similar to our proposed kinematics) is about $T = 0.43, 0.37$, and 0.36 for ^{40}Ca, ^{48}Ca, and ^{54}Fe, respectively. This difference is consistent with the expected variation of the opacity (equals one minus the transparency) as $A^{1/3}$.

For a given nucleus, protons with large and small p_{miss} have the same measured transparency [67]. Therefore the ratio of the large p_{miss} to small p_{miss} cross sections for a given nucleus should be independent of FSI.

The ratios of high-momentum protons in ^{40}Ca to ^{48}Ca and in ^{54}Fe to ^{48}Ca will need to be corrected for FSI. We will calculate the small change in the transparency from ^{54}Fe to ^{48}Ca and from ^{48}Ca to ^{40}Ca and compensate the data for it. In addition, we will construct an artificial, approximately $N = Z$ nucleus by averaging the results for ^{40}Ca and ^{54}Fe. Since the transparency of $(^{40}\text{Ca} + {}^{54}\text{Fe})/2$ and ^{48}Ca should be very similar, the ratio of high momentum protons in $(^{40}\text{Ca} + {}^{54}\text{Fe})/2$ to ^{48}Ca should be almost independent of FSI.

D. Impact on the 12 GeV JLab program

The results of this proposed measurement will complement other 12 GeV JLab experiments, particularly measurements of the spectral function of ^{40}Ar, inclusive quasielastic (e, e') measurements of nuclei at $x > 1$, and inclusive deep inelastic (e, e') measurements of nuclei at $x < 1$ (EMC effect).

E12-14-012 recently measured electro-induced proton knockout from ^{40}Ar and ^{48}Ti, to extract its mean-field spectral function (i.e., its single-nucleon properties and spectroscopic factors). They measured the missing momentum distribution of the cross section for the different mean-field orbitals (e.g. for Argon $1s_{1/2}, 2s_{1/2}, 1p_{1/2}, 1p_{3/2}, 1d_{3/2}$ and $1d_{5/2}$). Our measurement will focus instead on the knockout of high-momentum protons belonging to short range correlated pairs. We will measure the absolute cross-section as a function of missing momentum and energy and extract the distorted spectral function in kinematics where FSI are minimal. We will also studying how the number of SRC pairs changes when we change the number of neutrons and then the number of protons in the nucleus. Our measurement of SRC protons will thus complement E12-14-012's measurement of primarily mean-field protons.

E12-06-105 will measure inclusive electron scattering (e, e') on a wide variety of nuclei at $1.4 < x$ and $Q^2 \leq 5$ GeV^2 to extend previous studies of short range correlations in few-body and heavy nuclei. As shown in section **??**, inclusive cross section measurements alone cannot distinguish between electron scattering from a proton or from a neutron and thus cannot provide detailed information on the isospin assymetry dependence of SRCs. By studying how the number of high-momentum protons changes when we change the number of neutrons and then the number of protons in the nucleus, our experiment will provide complementary information that, together with the inclusice (e, e') measurements can be compared to detailed ab-inito calculations.

E12-10-108 will measure the EMC effect in inclusive deep inelastic (e, e') measurements of nuclei at $x < 1$. By comparing their measurements of the EMC effect to the SRC ratios measured at $x > 1.4$ in E12-06-105, they will extend our understanding of the EMC-SRC correlation. Their measurements off asymmetric nuclei also set to provide initial indications on the isospin dependence of the EMC effect. By studying the details of proton-neutron pairing, our experiment will provide complementary information needed to constrain both the standard nuclear effects contributing to the EMC ratios and the contribution of high-momentum (high-virtuality) nucleons to calculations of the average bound nucleon modification.

Along the same lines, Proposal PR12-14-007, "Constraints on Isovector-Dependent Nuclear Modification Effects Using Parity-Violating Deep Inelastic Scattering, seeks to measure the flavor-dependent nuclear medium modification (i.e., the EMC effect) in ^{48}Ca. The ^{48}Ca nucleus is chosen to maximize isospin asymmetry effects in a relatively well controlled nuclear environment. As mentioned, many models of the EMC effect relate medium modification of the bound nucleon structure to the virtuality of the nucleons in the nucleus, which is dominated by SRC nucleons. As shown in this propsoal, if in ^{48}Ca SRC pairs are dominated by np-SRC pairs, protons will have larger probabality than neutrons to have high momentum which will naturally lead to an isospin dependent EMC effect. Observing the latter is the goal of PR12-14-007. This proposal and ours are complementary measurements that will shed light on the origin of the recent correlations between EMC and SRC pairs in nuclei and the isospin dependent EMC effect as an explanation to the NuTeV anomaly.

E. Previous Measurements

While there have been a number of $(e, e'p)$ experiments at Jefferson Lab [66, 68–79], they have almost all focused on measuring nuclear transparencies or single nucleon properties of nuclei (i.e., nucleon knockout from valence shells). Very few have measured $(e, e'p)$ at SRC kinematics. Some experiments focused on measuring the correlated partner of the knocked-out proton [6, 8, 80]. However, these experiments measured nucleon knockout from symmetric nuclei (He and C) and were thus insensitive to the effects on the proton momentum distribution of adding neutrons.

Both Rohe *et al* [77] and Benmokhtar *et al* [66] measured $(e, e'p)$ over a wide range of missing energy and missing momentum to look for the effects of correlations. Benmokhtar measured the ^{3}He$(e, e'p)$ cross section in perpendicular kinematics (where the missing momentum and hence the undetected nucleon is perpendicular to the momentum transfer) and thus their cross sections in the correlations region are dominated by nucleon rescattering. Rohe *et al.* extracted the nuclear spectral function as a function of E_{miss} for three different values of p_{miss} in parallel kinematics [77]. They compared the measured spectral function to calculations, finding reasonable agreement only at $p_{miss} \approx 250$ MeV/c. They were interested in observing the existence of the correlated part of the spectral function. Our experiment will study in detail how the correlated part changes from ^{40}Ca to ^{48}Ca to ^{54}Fe.

The overall proportion of high momentum nucleons in various nuclei has been extracted from per-nucleon ratios of $A(e, e')$ to $d(e, e')$ cross sections. This has been measured for nuclei from ^{3}He to Au. Our measurement will complement the inclusive (e, e') measurement, shown in figure 9, since it is only sensitive to protons.

This will be the first $(e, e'p)$ measurement at Jefferson Lab to investigate the effects on nucleon SRC pairing of adding neutrons and protons in medium to heavy nuclei.

TABLE I: Proposed kinematics of the beam time for the measurement.

$E_{\rm Beam}$ GeV	E'_e GeV	θ_e	$\lvert\mathbf{p}_p\rvert$ GeV/c	θ_p	p_{miss} GeV/c	Q^2 GeV^2
11	9.85	8.0°	1.43	63.0°	0.40	2.1
11	9.85	8.0°	2.01	44.5°	0.15	1.8

III. THE PROPOSED MEASUREMENT

We will measure the absolute and reduced $(e,e'p)$ cross section on d, ^{4}He, ^{9}Be, ^{10}B, ^{11}B, ^{12}C, ^{28}Si, ^{40}Ar, ^{48}Ti, ^{40}Ca, ^{48}Ca, and ^{54}Fe at high and low missing momentum at large Q^2 and non-perpendicular kinematics. For the high p_{miss} kinematics we chose $Q^2 \approx 2$ GeV^2 to minimize the effects of Meson Exchange Currents and Isobar Configurations (Δ production). We chose $\theta_{rq} < 40°$ to minimize the effects of Final State Interactions at large missing momentum. This reduces the energy transfer and thus gives $x = Q^2/2m\nu > 1$, also reducing the effects of MEC and IC. Furthermore, we will measure $(e,e'p)$ on hydrogen for calibration purposes.

We will extract the relative probability for a proton to be at high-p_{miss} ($p_{miss} > p_{Fermi} \approx 250$ MeV/c) by calculating the ratio of the integrated cross section for high-p_{miss} to low-p_{miss} in each of the nuclei. The following ratios will be constructed:

- single ratios of high to low momentum protons in each of the nuclei,
- single ratios of high-momentum protons in heavier nuclei to deuterium,
- double ratios of high to low momentum protons in heavy nuclei relative to deuterium, C and, especially, ^{40}Ca relative to ^{48}Ca, and in ^{54}Fe relative to ^{48}Ca.

The first and third ratios will be independent of FSI. The second will be corrected for the change in transparency among the various nuclei. Note that there is only a small change in transparency between ^{40}Ca and ^{54}Fe.

We will use an 11 GeV beam and measure the scattered electron in the SHMS and the knocked out proton in the HMS. The SHMS will operate at a scattering angle of 8°.

We will use the existing Jefferson Lab 0.5-cm thick, 0.775 g/cm^2 ^{48}Ca target, along with similar ^{40}Ca, ^{54}Fe and other solid targets. Most of the solid targets can take at least 40 μA of beam; the B, C, ^{48}Ti and d targets can take up to 80 μA. [81]. For the cyro targets we will use the standard cells which are available. In case of ^{40}Ar the beam current is limited to 25 μA and the ^{40}Ar target can not be used in parallel to d and He due to the different cooling configurations [81].

The proposed kinematics are shown in Table I. The settings for the proton arm are determined by means of optimizing simulations with open acceptance and constraints on p_{miss}.

A. From cross section to ratios

As described in Section II B, we will measure the $(e,e'p)$ cross section at high- and low-p_{miss} on d and the other nuclei. We will extract the distorted spectral function using Eq. 10, correct it for the effects of FSI using the Glauber approximation [82], and correct it for the limited p_{miss}-dependent geometrical acceptance. We will then integrate the cross section over missing energy (up to π-emission threshold) and missing momentum. The low-p_{miss} bin will be integrated from 0 to 250 MeV/c and the high-p_{miss} bin will be integrated from about 350 to 550 MeV/c.

We will then construct the ratio of high-p_{miss} to the sum of low- and high-p_{miss} protons for each nucleus. These ratios will give the fraction of high momentum protons, and hence the protons belonging to SRC-pairs in each nucleus. We will compare these single-ratios to calculations of the proportions of high-momentum protons in the different nuclei. The effects of FSI should largely cancel in these ratios.

We will then construct the double ratios of high-p_{miss} to the sum of low- and high-p_{miss} protons for pairs of nuclei. The effects of FSI, ambiguities in the off-shell electron-proton cross section, and the geometrical extrapolation should all cancel in this double ratio.

B. Rate Estimates

To calculate the expected rates for this experiment at low-p_{miss} we used SIMC with spectral functions for the appropriate nuclei, scaled by their calculated transparencies. In the absence of realistic high-p_{miss} nuclear spectral

kinematics	SHMS acceptance cuts			HMS acceptance cuts			p_{miss}	x_B	θ_{rq}
	θ (in-plane)	ϕ	$\delta(p_e)/p_e$	θ	ϕ	$\delta(p_p)/p_p$	[MeV/c]		[°]
high-p_{miss}	±24mrad	±4mrad	$-0.1/+0.22$	±28mrad	±6mrad	±0.09	> 350	> 1.2	$< 40°$
low-p_{miss}							< 250	-	-

TABLE II: Selection cuts for the rate estimations from the simulated data. The cuts for both kinematical settings are given.

functions for heavy nuclei, we estimated the high-p_{miss} rates for this experiment in two ways: First, we extrapolated the rates from the $(e, e'p)$ measurement in Hall-A on a C-target (experiment E01-015) with similar momentum transfer [79, 80]. Second, we are using the deuterium momentum distribution as a proxy for the high-p_{miss} distribution in SIMC since they have the same shape, and the per-nucleon magnitude was measured by Refs. [5, 61]. We ran simulations of E01-015 and this experiment and scaled the E01-015 yield by the simulation ratio after correction of nuclear transparency and a_2 since the deuterium momentum distribution is used in the simulation.

For both kinematics we ran SIMC in the following configuration:

1. electrons detected at the SHMS, protons at the HMS.
2. Beam dimensions $89 \times 42 \mu m^2$.
3. Collimator in place.
4. Total beam charge 1.152 C, equivalent to a single 8-hour shift with a beam current of 40 μA.
5. The proposed kinematical settings with $E_{\text{Beam}} = 11$ GeV (see Table I).
6. liquid "deuterium" target characteristics:
   (a) ^{40}Ca density 1.55 g/cm^3.
   (b) Target length 0.5 cm - areal density of 0.775 g/cm^2).

For the rate estimations we applied additional cuts on the simulation results to account for spectrometer acceptances and kinematical cuts which will be used in the experimental analysis. The overview of the applied cuts for the two kinematical settings is shown in Table II.

1. *Low missing momentum kinematics*

For low missing momentum, the spectral functions for heavy nuclei exist, allowing SIMC to make reasonable rate estimates. Therefore, the simulation was performed using the standard SIMC ^{56}Fe mean-field spectral function with the same luminosity conditions, HMS and SHMS fiducial cuts as for the high-p_{miss} setting. After taking into account transparency and inefficiency, we estimate 40,000 events/hour for this kinematics (see Figs. 14 and 15 for the predicted kinematic variables distributions.). The estimations for the other targets have been obtained by scaling with their transparency and available beam current compared to Fe.

2. *High missing momentum kinematics*

The JLab experiment E01-015 ran in Hall-A and measured the ^{12}C$(e, e'p)$ reaction at $Q^2 = 2$ and $x_B = 1.2$, covering the same high missing momentum range of 350 – 550 MeV/c [79, 80]. First, we approximately extrapolated that measurement to this one as follows: We scaled their event rate to the luminosity of this proposal, to get an event rate of 1250 events per shift. Due to the smaller electron angle the Mott cross-section times the proton form factor squared increased the rate by about a factor of five. The considerably larger momentum acceptance of the Hall C spectrometers increase the effective acceptance by about a factor of two, leading to a total of about 12000 events per shift.

We quantified this acceptance increase by performing SIMC simulations using the AV18 deuteron momentum distribution for the kinematics of E01-015 for the spectrometers in Hall A and Hall C. The simulations for E01-015 result in kinematical distributions which matched the experimental ones, thus demonstrating the applicability of using the deuteron momentum distribution for heavier nuclei.

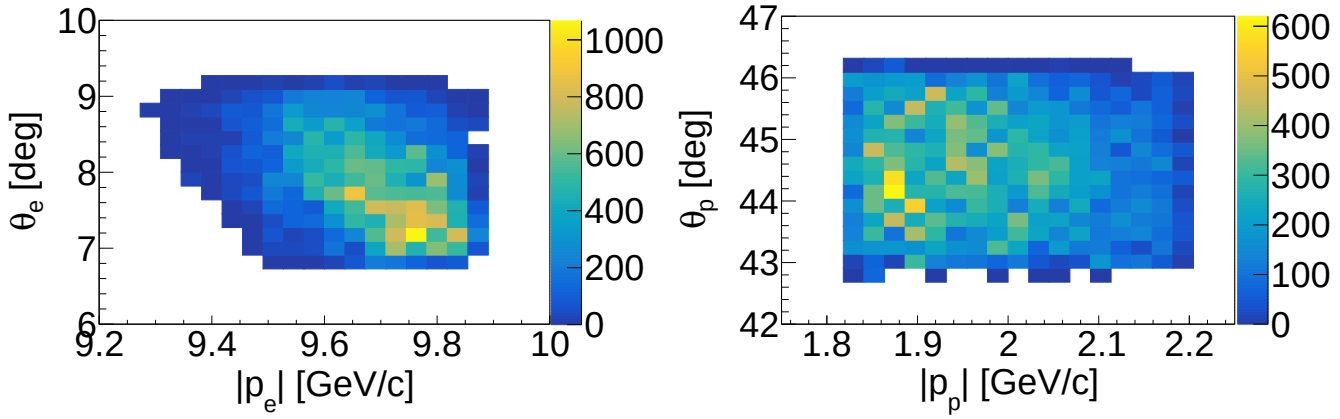

FIG. 14: The angle versus the momentum for the electron detected in the SHMS (left) and the proton detected in the HMS (right) for low missing momentum kinematics with cuts as described in Table II.

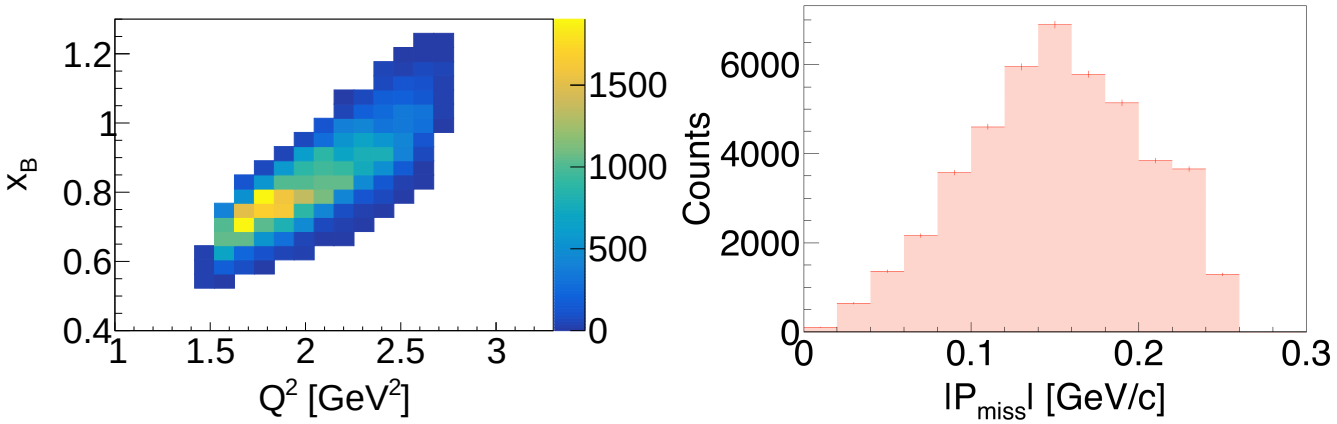

FIG. 15: On the left the x_B scaling variable versus the momentum transfer, Q^2 is shown. On the right, the expected missing momentum distribution is shown for the low-p_{miss} kinematics.

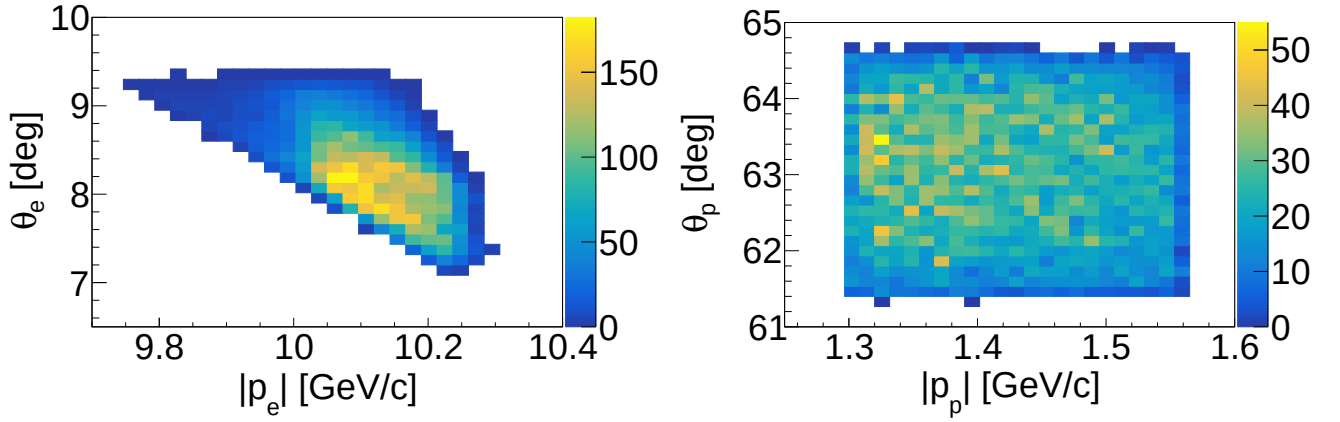

FIG. 16: The angle versus the momentum for the electrons detected in the SHMS (left) and the protons detected in the HMS (right) with cuts as described in Table II for the high-p_{miss} kinematics.

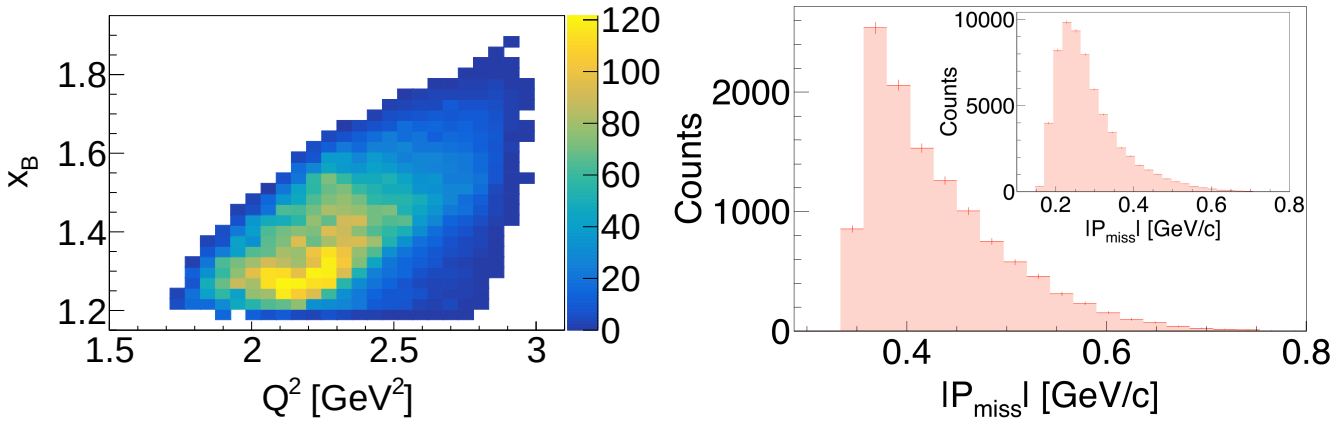

FIG. 17: On the left, the x_B scaling variable versus the momentum transfer, Q^2 is shown. On the right, the expected missing momentum for the high-p_{miss} kinematics is shown with the cuts from Table II. The inlay shows the missing momentum distribution without the cut on $p_{miss} > 350\,\mathrm{MeV/c}$.

We ran SIMC for the kinematics and acceptances of this experiment. To get the expected number of high-p_{miss} events in this experiment, we scaled the measured number of events for E01-015 by the ratio of the number of simulated events for this experiment and E01-015. This scaling give an event rate consistent with the ballpark estimate described above. The expected kinematical distributions after scaling and all cuts are shown in Figs. 16 and 17.

To determine the event rate for each target, we scaled the rate for ^{40}Ca by the transparencies, a_2 values, available beam currents and target areal densities of the other nuclei. In the end, we adjusted the beam time hours to get about 12000 events per target at the high-p_{miss} kinematics.

This event rate will allow us to make very precise ($\approx 2\%$) measurements of the high-p_{miss} to low-p_{miss} ratio and to study the behavior of the ratio as a function of p_{miss}.

The expected statistical uncertainties for the reduced cross sections integrated over missing energy as a funtion of missing momentum are shown in Figure 18. The plot was obtained by combining the scaled simulation results from the low and high-p_{miss} kinematics divided by the single nucleon off-shell cross sections σ_{cc2} [64].

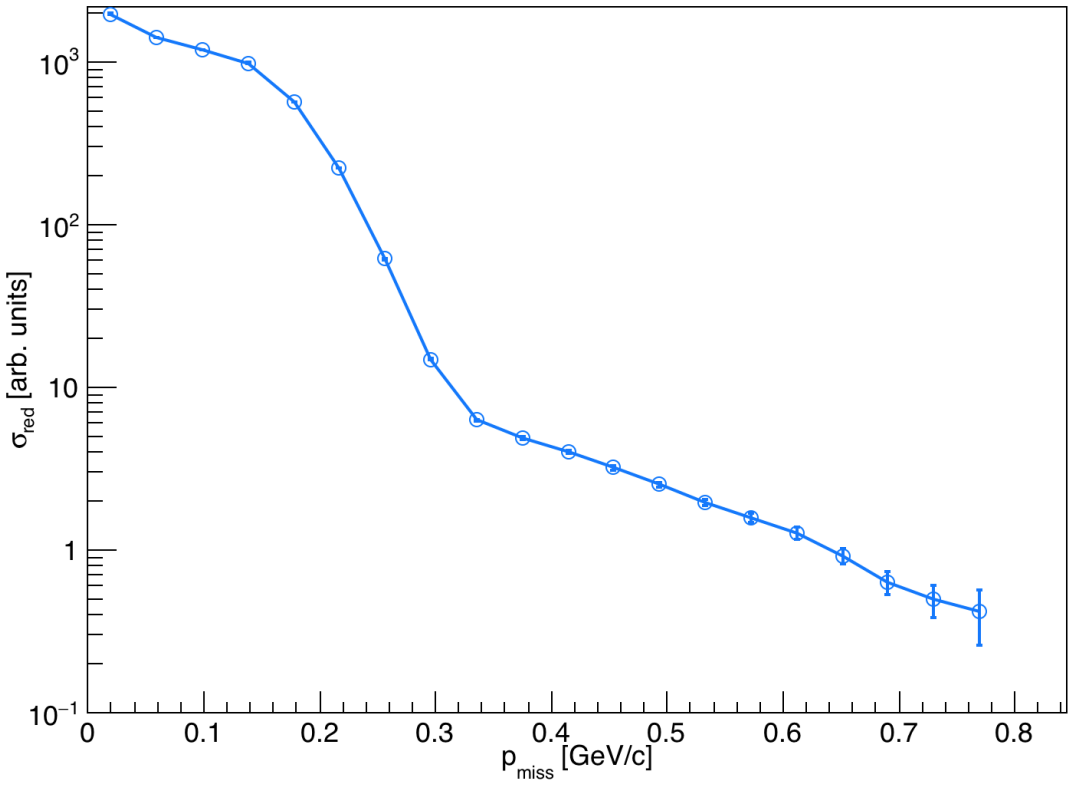

FIG. 18: The reduced cross section integrated over missing energy as a function of missing momentum with the expected statistical uncertainty determined from the above mentioned SIMC simulations for both kinematical settings.

kinematics	Target	Data-Taking [Hours]	Current [uA]	Expected Number [a] of Events
high p_{miss}	d, ^{4}He, ^{9}Be, ^{10}B, ^{11}B, ^{12}C,	42	40	12,000/target
	^{40}Ar	18	25	
	^{28}Si, ^{48}Ti, ^{40}Ca, ^{48}Ca, ^{54}Fe	45	40	
low p_{miss}	All Targets	18	25–40	>45,000/target
Commissioning and calibrations		15	20–60	
Target and spectrometer changes		30	N/A	
Total beam time		168 (7 days)		

[a]Dead time and detector efficiencies have been taking into account.

TABLE III: Requested beam time for each kinematic setting, target and spectrometer changes, calibrations and commissioning. In the high-p_{miss} kinematics the times are equally distributed for each target.

IV. BEAM TIME REQUEST AND EXPECTED RESULTS

This experiment requires 30 hours for target and spectrometer changes, 15 hours for commissioning and calibrations, 18 hours for the low-p_{miss} measurements on the eleven targets, and 105 hours for the high-p_{miss} measurements on the targets (as shown in Table III). The request for the target and spectrometer changes is more than one day since we expect a target swap during our beam time due to the different cryotargets. This swap usually needs one full day. We will also take elastic hydrogen data for calibration.

In total, we request 7 days of beamtime in Hall-C using the HMS and SHMS in their standard configurations with 11 GeV beam and 40 μA on all targets beside ^{40}Ar which can only be measured with 25 μA. We will require a short period during the calibration time with a higher current, approximately 60 μA, for current calibrations and boiling tests.

Based on similar experiments [83], we expect a $\approx$ 5% systematic uncertainty in the total cross section, including effects from acceptance corrections, radiative corrections, PID efficiency, charge measurement, target thickness, nuclear transparency etc. Most of these uncertainties will cancel when we construct ratios of cross sections. We conservatively expect that the remaining systematic uncertainties in the single ratios will be about 2–3% and the remaining systematic uncertainties in the double ratios (the ratio of high-p_{miss} to low-p_{miss} on one nucleus to that for a second nucleus) will be 1–2%.

The primary results of this measurement will be absolute cross sections and cross section ratios. We will construct the ratios of high-p_{miss} to the sum of low- and high-p_{miss} protons for each nucleus to determine the relative probability of high-p_{miss} protons in each nucleus. We will then construct the ratio of the relative probability of high-p_{miss} protons in each nucleus relative to the other nuclei. The effects of FSI, ambiguities in the off-shell electron-proton cross section, and the geometrical extrapolation should all cancel in this double ratio. These double ratios should correspond to the relative amounts of high-momentum protons in the different nuclei.

We expect to measure the ratios of the relative amounts of high-momentum protons in the different nuclei to 2–3%. This will let us distinguish precisely among the different pairing models.

V. SUMMARY

We propose to measure the $A(e,e'p)$ reaction for a series of specifically chosen target nuclei in both mean field and SRC kinematics, with the goal of significantly increasing our understanding of how protons and neutrons form short-range correlated pairs in nuclei. Our proposed targets can be divided into two groups:

1. ^{2}H, ^{4}He, ^{10}B, ^{12}C, ^{28}Si, ^{40}Ar are chosen to study the dependence of SRC pairing on nuclear mass,
2. ^{9}Be-^{10}B-^{11}B and ^{40}Ca-^{48}Ca-^{48}Ti-^{54}Fe are chosen to study the dependence on proton-neutron asymmetry.

Data will be collected for each target in both high-p_{miss} and low-p_{miss} kinematics to select mean field and SRC protons respectively. From this data, we will extract absolute and reduced cross-sections as a function of missing momentum and energy, constraining the distorted nuclear spectral function. We will also form the following ratios:

- the ratio of high-momentum protons to low-momentum protons in each of the target nuclei,
- the ratio of high-momentum protons in each nucleus to high-momentum protons in a reference nucleus (i.e., ^{2}H, ^{12}C, etc.)
- the double ratio of the above two.

Results from a recent Hall B data-mining analysis show the effectiveness of the above mentioned ratio method in minimizing FSI effects.

These ratios have a number of important implications. First and foremost, from these ratios, we can infer the fraction of protons that form SRC pairs in the different target nuclei. The targets chosen will allow unprecedented study of the mass and isospin dependence of the SRC pairs fractions. Second, the range of different nuclear masses can test theories of final state interactions and transparency corrections. Third, the study of the ^{9}Be-^{10}B-^{11}B triplet and ^{40}Ca-^{48}Ca-^{48}Ti-^{54}Fe quartet will give insight to the formation mechanism of SRC pairs, especially between protons in different angular momentum orbitals.

This comprehensive data-set, combined with results from inclusive (e,e') ratios, will be used to extract high-momentum pairing probabilities that can be compared to ab-initio calculations of one body momentum densities, and to constrain nuclear contacts that can be compared to ab-initio based extractions from two-body momentum and coordinate space densities.

This measurement has the potential to make definitive impacts in many different areas, and we highlight three:

1. the origin of the EMC effect and, specifically, its isospin-dependence which is relevant to the NuTeV anomaly.
2. the effect of SRC pairing on the nuclear symmetry energy, especially at supra-nuclear density
3. cross sections and distributions in multi-nucleon knock-out in neutrino-nucleus scattering

We therefore request 7 days of 11 GeV beam time in Hall C for this measurement.

VI. APPENDIX I: RESPOND TO THE REPORT OF THE 44TH PROGRAM ADVISORY COMMITTEE (PAC44)

Issues: While the area of induced correlations due to short range part of the nucleon-nucleon interaction is of interest, the PAC found the proposal lacking in details. For example, a future proposal should give concrete theoretical calculations of how SRC affect physics. Rather than state that SRC pairs will affect neutrino-nucleus interactions, how does the counting of pairs discriminate among modern theories of the nuclear interactions?

The revised proposal now refers to three concrete quantitative examples that show how SRC affect physics (for details see pages 5 – 8). These include:

- The value of the nuclear symmetry energy at supra-nuclear densities,
- Cross sections, multi-nucleon knockout, and distorted spectral functions in quasi-elastic neutrino-nucleus scattering.
- The EMC effect and its isospin dependence.

It should be noted that the proposed measurements will provide valuable information needed to better constrain the above mentioned and other calculations. Specifically, in the case of the EMC effect, the proposed extraction of proton and neutron pairing probabilities will constrain not only the contribution of 'traditional' nuclear physics effects on the measured DIS cross-section ratios, but also the relative strength that SRC-inspired models can assign to medium-modification when fitting world EMC data.

What are the quantities that theorists could calculate using modern nucleon interactions (e.g., AV18 plus three nucleon potentials and others) and experimentalists could measure that would distinguish among the interactions on the market?

The amount of protons and neutrons in the high momentum tail of asymmetric nuclei such as ^{11}B and ^{48}Ca are quantities that can both be calculated using state-of-the-art theoretical techniques, and be extracted in the proposed measurement. Different calculations of the one-body momentum density vary significantly at high momenta (see for example the difference between CC and VMC calculation based on the N2LO$_{SAT}$ and AV18+UIX interactions respectively, shown in Fig. 11). Details are given on page 10 and 11.

Recent advances in effective theories such as the Contact formalism were shown to provide a bridge between experimentaly measured cross-sections and cross-section ratios and ab-initio two-body densities [19]. Both experimental data and theretical calculations are sensitive to the same contacts, allowing for a detailed comparison.

[1] L. Lapikas, Nuclear Physics A **553**, 293c (1993).
[2] G. Kramer, H. Blok, and L. Lapiks, Nuclear Physics A **679**, 267 (2001), ISSN 0375-9474, URL http://www.sciencedirect.com/science/article/pii/S0375947400003791.
[3] K. Egiyan et al. (CLAS Collaboration), Phys. Rev. C **68**, 014313 (2003).
[4] K. Egiyan et al. (CLAS Collaboration), Phys. Rev. Lett. **96**, 082501 (2006).
[5] N. Fomin et al., Phys. Rev. Lett. **108**, 092502 (2012).
[6] R. Subedi et al., Science **320**, 1476 (2008).
[7] E. Piasetzky, M. Sargsian, L. Frankfurt, M. Strikman, and J. W. Watson, Phys. Rev. Lett. **97**, 162504 (2006).
[8] I. Korover, N. Muangma, O. Hen, et al., Phys.Rev.Lett. **113**, 022501 (2014), 1401.6138.
[9] M. Alvioli, C. C. degli Atti, and H. Morita, Phys. Rev. Lett. **100**, 162503 (2008).
[10] R. Schiavilla, R. B. Wiringa, S. C. Pieper, and J. Carlson, Physical Review Letters **98**, 132501 (2007).
[11] M. M. Sargsian, T. V. Abrahamyan, M. I. Strikman, and L. L. Frankfurt, Phys. Rev. C **71**, 044615 (2005).
[12] O. Hen, M. Sargsian, L. B. Weinstein, E. Piasetzky, H. Hakobyan, D. W. Higinbotham, M. Braverman, W. K. Brooks, S. Gilad, K. P. Adhikari, et al. (CLAS Collaboration), Science **346**, 614 (2014).
[13] D. Lonardoni, A. Lovato, S. C. Pieper, and R. B. Wiringa (2017), 1705.04337.
[14] J. Carlson, S. Gandolfi, F. Pederiva, S. C. Pieper, R. Schiavilla, K. E. Schmidt, and R. B. Wiringa, Rev. Mod. Phys. **87**, 1067 (2015), 1412.3081.
[15] G. Hagen, G. R. Jansen, and T. Papenbrock, Phys. Rev. Lett. **117**, 172501 (2016), 1605.01477.
[16] R. F. Garcia Ruiz et al., Nature Phys. **12**, 594 (2016), 1602.07906.
[17] G. Hagen et al., Nature Phys. **12**, 186 (2015), 1509.07169.
[18] A. Bulgac, M. M. Forbes, and S. Jin (2015), 1506.09195.
[19] R. Weiss, R. Cruz-Torres, N. Barnea, E. Piasetzky, and O. Hen (2016), 1612.00923.
[20] M. Alvioli, C. Ciofi degli Atti, and H. Morita, Phys. Rev. **C94**, 044309 (2016), 1607.04103.
[21] C. Ciofi degli Atti, C. B. Mezzetti, and H. Morita, Phys. Rev. **C95**, 044327 (2017), 1701.08211.
[22] J. Ryckebusch, W. Cosyn, and M. Vanhalst, J. Phys. **G42**, 055104 (2015), 1405.3814.
[23] A. Carbone, A. Polls, and A. Rios, Euro. Phys. Lett. **97**, 22001 (2012).
[24] I. Vidaña, A. Polls, and C. m. c. Providência, Phys. Rev. C **84**, 062801 (2011), URL http://link.aps.org/doi/10.1103/PhysRevC.84.062801.
[25] C. Xu, A. Li, and B. Li, J. of Phys: Conference Series **420**, 012190 (2013).
[26] C. Xu and B. Li (2011), 1104:2075.
[27] J. M. Lattimer and Y. Lim, Apj **771**, 51 (2013).
[28] O. Hen, B.-A. Li, W.-J. Guo, L. B. Weinstein, and E. Piasetzky, Phys. Rev. C **91**, 025803 (2015), URL http://link.aps.org/doi/10.1103/PhysRevC.91.025803.
[29] G. A. Fiorentini et al. (MINERvA Collaboration), Phys. Rev. Lett. **111**, 022501 (2013).
[30] G. A. Fiorentini et al. (MINERvA Collaboration), Phys. Rev. Lett. **111**, 022502 (2013).
[31] L. B. Weinstein, E. Piasetzky, D. W. Higinbotham, J. Gomez, O. Hen, and R. Shneor, Phys. Rev. Lett. **106**, 052301 (2011).
[32] O. Hen, E. Piasetzky, and L. B. Weinstein, Phys. Rev. C **85**, 047301 (2012).
[33] L. Frankfurt and M. Strikman, Phys. Rep. **160**, 235 (1988).
[34] O. Hen et al., Int. J. Mod. Phys. E **22**, 133017 (2013).
[35] G. P. Zeller et al., Phys. Rev. Lett. **88**, 091802 (2002), URL http://link.aps.org/doi/10.1103/PhysRevLett.88.091802.
[36] I. C. Cloët, W. Bentz, and A. W. Thomas, Phys. Rev. Lett. **102**, 252301 (2009), URL http://link.aps.org/doi/10.1103/PhysRevLett.102.252301.
[37] F. Šimkovic, A. Faessler, H. Müther, V. Rodin, and M. Stauf, Phys. Rev. C **79**, 055501 (2009), URL http://link.aps.org/doi/10.1103/PhysRevC.79.055501.
[38] M. Kortelainen and J. Suhonen, Phys. Rev. **C75**, 051303 (2007), 0705.0469.
[39] L. Frankfurt, M. Sargsian, and M. Strikman, International Journal of Modern Physics A **23**, 2991 (2008), http://www.worldscientific.com/doi/pdf/10.1142/S0217751X08041207, URL http://www.worldscientific.com/doi/abs/10.1142/S0217751X08041207.
[40] D. J. Dean and M. Hjorth-Jensen, Rev. Mod. Phys. **75**, 607 (2003), nucl-th/0210033.
[41] B.-J. Cai and B.-A. Li (2017), 1703.08743.
[42] B.-J. Cai and B.-A. Li, Phys. Rev. **C93**, 014619 (2016), 1509.09290.
[43] T. Van Cuyck, N. Jachowicz, R. Gonzlez-Jimnez, M. Martini, V. Pandey, J. Ryckebusch, and N. Van Dessel, Phys. Rev. **C94**, 024611 (2016), 1606.00273.
[44] *"int workshop, neutrino-nucleus interactions for current and next generation neutrino oscillation experiments (int-13-54w)."*.
[45] C. M. Jen, A. Ankowski, O. Benhar, A. P. Furmanski, L. N. Kalousis, and C. Mariani, Phys. Rev. **D90**, 093004 (2014), 1402.6651.
[46] O. Hen, G. Miller, E. Piasetzky, and L. B. Weinstein, submitted to Rev. Mod. Phys. (2016), 1611.09748.
[47] D. Geesaman, K. Saito, and A. Thomas, Ann. Rev. Nucl. and Part. Sci. **45**, 337 (1995).
[48] P. R. Norton, Rep. Prog. Phys. **66**, 1253 (2003).
[49] L. Frankfurt and M. Strikman, Phys. Rev. C **82**, 065203 (2010).

[50] S. A. Kulagin and R. Petti, Nucl. Phys. A **765**, 126 (2006).
[51] S. A. Kulagin and R. Petti, Phys. Rev. C **82**, 054614 (2010).
[52] J. Arrington, D. Higinbotham, G. Rosner, and M. Sargsian, Progress in Particle and Nuclear Physics **67**, 898 (2012), ISSN 0146-6410, URL http://www.sciencedirect.com/science/article/pii/S0146641012000749.
[53] O. Hen, L. Weinstein, S. Wood, and S. Gilad, *In Medium Nucleon Structure Functions, SRC, and the EMC effect, Jefferson Lab experiment E12-11-107* (2011).
[54] O. Hen, L. Weinstein, E. Piasetzky, and H. Hakobyan, *In Medium Proton Structure Functions, SRC, and the EMC effect, Jefferson Lab experiment E12-11-003A* (2015).
[55] J. R. Smith and G. A. Miller, Phys. Rev. **C65**, 055206 (2002), nucl-th/0202016.
[56] C. Ciofi degli Atti and S. Liuti, Phys. Rev. **C44**, R1269 (1991).
[57] A. E. L. Dieperink and G. A. Miller, Phys. Rev. **C44**, 866 (1991).
[58] L. Frankfurt and M. Strikman, Int. J. Mod. Phys. **E21**, 1230002 (2012), 1203.5278.
[59] O. Hen, D. W. Higinbotham, G. A. Miller, E. Piasetzky, and L. B. Weinstein, Int. J. Mod. Phys. **E22**, 1330017 (2013), 1304.2813.
[60] I. C. Cloet, W. Bentz, and A. W. Thomas, Phys. Lett. **B642**, 210 (2006), nucl-th/0605061.
[61] Z. Ye, Ph.D. thesis, University of Virginia (2013), 1408.5861.
[62] J. Carlson and S. Gandolfi, Private communication.
[63] J. Kelly, Adv. Nucl. Phys. **23**, 75 (1996).
[64] T. De Forest, Nucl. Phys. **A392**, 232 (1983).
[65] M. Sargsian, *Private communication.*
[66] F. Benmokhtar et al. (Jefferson Lab Hall A Collaboration), Phys. Rev. Lett. **94**, 082305 (2005).
[67] O. Hen et al. (CLAS Collaboration), Phys.Lett. **B722**, 63 (2013), 1212.5343.
[68] K. Garrow, D. McKee, A. Ahmidouch, C. S. Armstrong, J. Arrington, R. Asaturyan, S. Avery, O. K. Baker, D. H. Beck, H. P. Blok, et al., Phys. Rev. C **66**, 044613 (2002), URL http://link.aps.org/doi/10.1103/PhysRevC.66.044613.
[69] K. Fissum et al. (Jefferson Lab Hall A Collaboration), Phys.Rev. **C70**, 034606 (2004), nucl-ex/0401021.
[70] J. Gao et al., Phys. Rev. Lett. **84**, 3265 (2000).
[71] N. Liyanage, B. D. Anderson, K. A. Aniol, L. Auerbach, F. T. Baker, J. Berthot, W. Bertozzi, P.-Y. Bertin, L. Bimbot, W. U. Boeglin, et al. (The Jefferson Lab Hall A Collaboration), Phys. Rev. Lett. **86**, 5670 (2001), URL http://link.aps.org/doi/10.1103/PhysRevLett.86.5670.
[72] J. Herraiz, Ph.D. thesis, Universidad Complutense de Madrid (2010).
[73] D. Dutta et al., Phys. Rev. C **68**, 064603 (2003), URL http://link.aps.org/doi/10.1103/PhysRevC.68.064603.
[74] J. Arrington, D. Higinbotham, G. Rosner, and M. Sargsian, Prog.Part.Nucl.Phys. **67**, 898 (2012), 1104.1196.
[75] M. M. Rvachev et al. (Jefferson Lab Hall A Collaboration), Phys. Rev. Lett. **94**, 192302 (2005).
[76] D. Rohe, O. Benhar, C. S. Armstrong, R. Asaturyan, O. K. Baker, S. Bueltmann, C. Carasco, D. Day, R. Ent, H. C. Fenker, et al. (E97-006 Collaboration), Phys. Rev. C **72**, 054602 (2005), URL http://link.aps.org/doi/10.1103/PhysRevC.72.054602.
[77] D. Rohe, C. S. Armstrong, R. Asaturyan, O. K. Baker, S. Bueltmann, C. Carasco, D. Day, R. Ent, H. C. Fenker, K. Garrow, et al. (E97-006 Collaboration), Phys. Rev. Lett. **93**, 182501 (2004), URL http://link.aps.org/doi/10.1103/PhysRevLett.93.182501.
[78] O. Hen, H. Hakobyan, R. Shneor, E. Piasetzky, L. Weinstein, W. Brooks, S. M.-T. Beck, S. Gilad, I. Korover, A. Beck, et al., Physics Letters B **722**, 63 (2013), ISSN 0370-2693, URL http://www.sciencedirect.com/science/article/pii/S0370269313002906.
[79] P. Monaghan, R. Shneor, R. Subedi, B. D. Anderson, K. Aniol, J. Annand, J. Arrington, H. B. Benaoum, F. Benmokhtar, P. Bertin, et al., Journal of Physics G: Nuclear and Particle Physics **41**, 105109 (2014), URL http://stacks.iop.org/0954-3899/41/i=10/a=105109.
[80] R. Shneor et al., Phys. Rev. Lett. **99**, 072501 (2007).
[81] D. Meekins, *Private communication* (2017).
[82] C. Colle, W. Cosyn, and J. Ryckebusch, *Final-state interactions in two-nucleon knockout reactions* (2015), 1512.07841.
[83] D. Dutta and R. Ent, *The Search for Color Transparency at 12 GeV, Jefferson Lab Experiment E12-06-107* (2006).